WATER RESOURCES RESEARCH, VOL. 46, W07508, doi:10.1029/2009WR008899, 2010

Improved forward and inverse analyses of saturated-unsaturated flow toward a well in a compressible unconfined aquifer

Phoolendra Kumar Mishra[1] and Shlomo P. Neuman[1]

Received 12 November 2009; revised 22 February 2010; accepted 4 March 2010; published 10 July 2010.

[1] We present an analytical solution for flow to a partially penetrating well in a compressible unconfined aquifer that allows inferring its saturated and unsaturated hydraulic properties from drawdowns recorded in the saturated and/or unsaturated zone. We improve upon a previous such solution due to Tartakovsky and Neuman (2007) by (1) adopting a more flexible representation of unsaturated zone constitutive properties and (2) allowing the unsaturated zone to have finite thickness. Both solutions account for horizontal as well as vertical flows throughout the system. We investigate the effects of unsaturated zone constitutive parameters and thickness on drawdowns in the saturated and unsaturated zones as functions of position and time; demonstrate the development of significant horizontal hydraulic gradients in the unsaturated zone in response to pumping; validate our solution against numerical simulations of drawdown in a synthetic aquifer having unsaturated properties described by the van Genuchten-Mualem constitutive model; use our solution to analyze drawdown data from a pumping test conducted by the U.S. Geological Survey at Cape Cod, Massachusetts; and compare our estimates of van Genuchten-Mualem parameters with laboratory values obtained for similar materials in the area.

Citation: Mishra, P. K., and S. P. Neuman (2010), Improved forward and inverse analyses of saturated-unsaturated flow toward a well in a compressible unconfined aquifer, *Water Resour. Res.*, *46*, W07508, doi:10.1029/2009WR008899.

1. Introduction

[2] *Tartakovsky and Neuman* [2007] developed an analytical solution for flow to a partially penetrating well pumping at a constant rate from a compressible unconfined aquifer considering an unsaturated zone of infinite thickness. In their solution three-dimensional, axially symmetric unsaturated flow was described by a linearized version of Richards' equation in which both relative hydraulic conductivity and water content vary exponentially with incremental capillary pressure head relative to a threshold (negative of air entry pressure head, $\psi_a \leq 0$). Both exponential functions were characterized by a common exponent κ having the dimension of inverse length, or equivalently a dimensionless exponent $\kappa_D = \kappa b$ where b is initial saturated thickness.

[3] A solution admitting two separate values of κ, one characterizing relative hydraulic conductivity and the other water content, was developed by *Mathias and Butler* [2006]. Whereas their solution allowed the unsaturated zone to have finite thickness, it considered flow in this zone to be strictly vertical. Though their paper did not consider explicitly flow to a partially penetrated well, they did note the possibility of accounting for it in principle by incorporating their "drainage function" in a solution considering a partially penetrating well of finite radius due to *Moench* [1997].

[4] Analyses by *Moench* [2008] have indicated a need to characterize relative hydraulic conductivity and water content by two separate exponents, in the manner of *Mathias and Butler* [2006]. The work of *Tartakovsky and Neuman* [2007] has demonstrated the development of significant horizontal hydraulic gradients within the unsaturated zone in response to pumping. Numerical simulations by *Moench* [2008] have likewise shown "flow … above the capillary fringe to be more horizontal than vertical." This has led *Moench* [2008] to conclude that extending the model of *Tartakovsky and Neuman* [2007] to include two separate exponents, finite unsaturated zone thickness and borehole storage would constitute a welcome addition to the aquifer-test literature.

[5] We present a new analytical solution that is similar in all respects to that of *Tartakovsky and Neuman* [2007] but characterizes relative hydraulic conductivity and water content by means of separate thresholds and exponents and allows unsaturated zone thickness to be finite. Our solution is not a direct extension of that by *Tartakovsky and Neuman* [2007], requiring instead a substantially different mathematical approach. By adding two free parameters to our representation of unsaturated hydraulic properties we are able to obtain better fits to standard constitutive models, most notably that of *van Genuchten* [1980] and *Mualem* [1976], than is possible with the three-parameter version of *Mathias and Butler* [2006] as demonstrated in Appendix A. Our solution further differs from the latter by allowing flow in the unsaturated zone to take place horizontally and by being self contained, coupling the unsaturated and saturated zones directly (the solution of Mathias and Butler, though restricted to the unsaturated zone, can be coupled

[1]Department of Hydrology and Water Resources, University of Arizona, Tucson, Arizona, USA.

0043-1397/10/2009WR008899

with that of *Moench* [1997] to include flow toward a partially penetrating well with storage in the saturated zone). We investigate the effects of unsaturated zone constitutive parameters and thickness on drawdowns in the saturated and unsaturated zones as functions of position and time. We then validate our solution against numerical simulations of drawdown in a synthetic aquifer having unsaturated properties described by the *van Genuchten* [1980]–*Mualem* [1976] model. We conclude by using our solution to analyze drawdown data from a pumping test conducted by *Moench et al.* [2001] in a glacial outwash deposit at Cape Cod, Massachusetts, and comparing our estimates of van Genuchten-Mualem parameters with laboratory values obtained for similar materials in the same area by *Mace et al.* [1998].

2. Theory

2.1. Statement of Problem and Linearization

[6] Like *Tartakovsky and Neuman* [2007, Figure 1] we consider a compressible unconfined aquifer of infinite lateral extent resting on an impermeable boundary. The aquifer is spatially uniform and anisotropic with a fixed ratio $K_D = K_z/K_r$ between vertical and horizontal saturated hydraulic conductivities, K_z and K_r, respectively. The aquifer is saturated beneath an initially horizontal water table at elevation $z = b$ defined as a $\psi = \psi_a$ isobar where ψ is pressure head and $\psi_a \le 0$ is the pressure head required for air to enter a saturated medium. A saturated capillary fringe at nonpositive pressure $\psi_a \le \psi \le 0$ extends from the water table down to the $\psi = 0$ isobar (traditional water table) at elevation $b + \psi_a$ (note that the capillary fringe disappears if one sets $\psi_a = 0$). Prior to the onset of pumping the saturated and overlying unsaturated zones are at uniform initial hydraulic head $h_0 = b + \psi_a$. Starting at time $t = 0$, water is withdrawn at a constant volumetric rate Q from a well of zero radius that penetrates the saturated zone between depths l and d below the initial water table (at air entry pressure). The system of equations governing flow in this system, given by Tartakovsky and Neuman, is highly nonlinear due to (1) the nonlinear nature of Richards' equation and (2) the presence of a moving interface (water table) between two different (saturated and unsaturated) flow regimes. To solve it the authors restrict consideration to a pumping rate Q that is small compared to $K_r b^2$, expand the dependent variables in power series and disregard terms of order higher than first in Q, as did *Kroszynski and Dagan* [1975]. Doing so while treating horizontal flux into a pumping well of zero radius as if it was vertically uniform led *Tartakovsky and Neuman* [2007] to the following first-order representation of flow in the saturated zone,

$$K_r \frac{1}{r}\frac{\partial}{\partial r}\left(r\frac{\partial s}{\partial r}\right) + K_z\frac{\partial^2 s}{\partial z^2} = S_s\frac{\partial s}{\partial t} \qquad 0 \le z < b \tag{1}$$

$$s(r,0) = b \text{ or } s_0 = 0 \tag{2}$$

$$s(\infty,z,t) = 0 \tag{3}$$

$$\frac{\partial s}{\partial z} = 0 \qquad z = 0 \tag{4}$$

$$\lim_{r\to 0} r\frac{\partial s}{\partial r} = 0 \qquad 0 \le z \le b-l \qquad b-d \le z \le b \tag{5}$$

$$\lim_{r\to 0} r\frac{\partial s}{\partial r} = -\frac{Q}{2\pi K_r(l-d)} \qquad b-l \le z \le b-d \tag{6}$$

where $s(r,z,t) = h_0 - \mathrm{h}(r,z,t)$ is drawdown, $h(r,z,t)$ being hydraulic head, and S_s is specific storage. To first order of approximation, Tartakovsky and Neuman described flow in the unsaturated zone via

$$K_r k_0(z)\frac{1}{r}\frac{\partial}{\partial r}\left(r\frac{\partial \sigma}{\partial r}\right) + K_z\frac{\partial}{\partial z}\left(k_0(z)\frac{\partial \sigma}{\partial z}\right) = C_0(z)\frac{\partial \sigma}{\partial t} \qquad b < z < b+L \tag{7}$$

$$k_0(z) = k(\theta_0) \qquad C_0(z) = C(\theta_0) \tag{8}$$

$$\sigma_0 = 0 \tag{9}$$

$$\sigma(\infty,z,t) = 0 \tag{10}$$

$$\frac{\partial \sigma}{\partial z} = 0 \qquad z = b+L \tag{11}$$

$$\lim_{r\to 0} r\frac{\partial \sigma}{\partial r} = 0 \qquad b < z < b+L \tag{12}$$

where $\sigma(r,z,t) = h_0 - h(r,z,t) = b + \psi_a - h(r,z,t)$ is drawdown in the unsaturated zone, L is the thickness of the unsaturated zone (whereas Tartakovsky and Neuman considered L to be infinite, we allow it to remain finite as did *Mathias and Butler* [2006]), $0 \le k(\psi) \le 1$ is relative (ratio of actual to saturated) hydraulic conductivity and $C(\psi) \ge 0$ is specific moisture capacity $C(\psi) = d\theta/d\psi$, θ being volumetric water content and the subscript 0 indicating initial conditions. The unsaturated and saturated zone flow regimes are coupled by interface conditions representing continuity of pressure and normal flux across the water table which, following linearization, take the form

$$s - \sigma = 0 \qquad z = b \tag{13}$$

$$\frac{\partial s}{\partial z} - \frac{\partial \sigma}{\partial z} = 0 \qquad z = b. \tag{14}$$

[7] Like *Tartakovsky and Neuman* [2007] we represent the aquifer water retention characteristics by means of an exponential function

$$S_e = \frac{\theta(\psi) - \theta_r}{S_y} = e^{a_c(\psi-\psi_a)} \qquad a_c \ge 0 \tag{15}$$

where S_e is effective saturation, θ_r is residual water content and $S_y = \theta_s - \theta_r$ is drainable porosity or specific yield. Like them we adopt *Gardner*'s [1958] exponential model for relative hydraulic conductivity,

$$k(\psi) = \begin{cases} e^{a_k(\psi-\psi_k)} & \psi \le \psi_k \\ 1 & \psi < \psi_k \end{cases} \qquad a_k \ge 0, \tag{16}$$

but with parameters a_k and ψ_k that may differ from a_c and ψ_a in (15). The parameter $\psi_k \leq 0$ represents a pressure head above which relative hydraulic conductivity is effectively equal to unity, which is sometimes but not always equal to the air entry pressure head ψ_a. Considering this latter possibility, our four-parameter representation of these functions allows more flexibility than the two-parameter representations of *Tartakovsky and Neuman* [2007] (a_c and ψ_a) or the three-parameter representation of *Mathias and Butler* [2006] (ψ_a, a_c and a_k). It implies that

$$k_0(z) = e^{a_k(b_1+b-z)} \qquad b_1 = \psi_a - \psi_k \tag{17}$$

$$C_0(z) = S_y a_c e^{a_c(b-z)} \tag{18}$$

in (7) and (8). Though the linearized solution thus depends only on the difference $b_1 = \psi_a - \psi_k$ between ψ_a and ψ_k, further fit of this solution to constitutive models of water retention and relative hydraulic conductivity such as those of *Gardner* [1958] and *Russo* [1988], *Brooks and Corey* [1964] or *van Genuchten* [1980] and *Mualem* [1976] allows, and may at times require, distinguishing between the two as we illustrate in Appendix A.

2.2. Point Drawdown in Saturated and Unsaturated Zones

[8] In a manner analogous to *Neuman* [1974] and *Tartakovsky and Neuman* [2007] we decompose drawdown in the saturated zone into two parts (Appendix B)

$$s = s_H + s_U \tag{19}$$

where s_H is *Hantush*'s [1964] solution for a partially penetrating well in a confined aquifer and s_U is a correction due to the presence of an unsaturated zone. Hantush's solution further decomposes into

$$s_H = s_T + \Delta s \tag{20}$$

where s_T is the *Theis* [1935] solution

$$s_T = \frac{Q}{4\pi T}\int_{1/4t_s}^{\infty} \frac{e^{-y}}{y}dy \tag{21}$$

and Δs is a correction due to partial penetration given by

$$\Delta s = \frac{Q}{4\pi T}\frac{2}{\pi(l_D-d_D)}\sum_{n=1}^{\infty}\frac{1}{n}\cos[n\pi(1-z_D)][\sin(n\pi l_D)-\sin(n\pi d_D)] \cdot \int_{1/4t_s}^{\infty}\exp\left[-y-\frac{K_D^{1/2}r_D(n\pi)^2}{4y}\right]\frac{dy}{y} \tag{22}$$

in which $T = K_r b$ is transmissivity, $t_s = \alpha_s t/r^2$ is dimensionless time with respect to the compressive hydraulic diffusivity $\alpha_s = K_r/S_s$, $r_D = r/b$, $z_D = z/b$, $l_D = l/b$ and $d_D = d/b$.

[9] We show in Appendices C and D that the Laplace transforms of s_U and σ are given by

$$\bar{s}_U(r_D, z_D, p_D) = \frac{Qt}{2\pi TK_D p_D}\int_0^{\infty}\frac{\cosh(\mu z_D)}{\cosh(\mu)-\frac{\mu}{qb}\sinh(\mu)} \cdot \frac{\sinh[\mu(1-l_D)]-\sinh[\mu(1-d_D)]}{\mu^2(l_D-d_D)\sinh(\mu)} yJ_0(yK_D^{1/2}r_D)\mathrm{d}y \tag{23}$$

and

$$\bar{\sigma}(r_D, z_D, p_D) = \begin{cases} \dfrac{Qt}{2\pi TK_D p_D}\displaystyle\int_0^{\infty} e^{a_{kD}(z_{D-1})/2}\left[\frac{\cosh(\mu)}{\cosh(\mu)-\frac{\mu}{qb}\sinh(\mu)}-1\right]\frac{J_n[i\phi(z_D-1)]+\chi Y_n[i\phi(z_D-1)]}{J_n[i\phi(0)]+\chi Y_n[i\phi(0)]} \\ \quad \cdot\dfrac{\sinh[\mu(1-l_D)]-\sinh[\mu(1-d_D)]}{\mu^2(l_D-d_D)\sinh(\mu)} yJ_0(yK_D^{1/2}r_D)\mathrm{d}y \quad \text{for } a_{cD} \neq a_{kD} \\ \dfrac{Qt}{2\pi TK_D p_D}\displaystyle\int_0^{\infty}\left[\frac{\cosh(\mu)}{\cosh(\mu)-\frac{\mu}{qb}\sinh(\mu)}-1\right]\frac{e^{\delta_{1D}(z_D-1)}+\chi e^{\delta_{2D}(z_D-1)}}{1+\chi} \\ \quad \cdot\dfrac{\sinh[\mu(1-l_D)]-\sinh[\mu(1-d_D)]}{\mu^2(l_D-d_D)\sinh(\mu)} yJ_0(yK_D^{1/2}r_D)\mathrm{d}y \quad \text{for } a_{cD} = a_{kD} = \kappa_D \end{cases} \tag{24}$$

respectively, where

$$p_D = pt,\ \mu^2 = y^2 + \frac{p_D}{t_s K_D r_D^2}, \qquad \phi(z_D) = \sqrt{\frac{4B_D}{\lambda_D^2}}e^{\lambda_D z_D/2},$$

$$\lambda_D = a_{kD} - a_{cD},\ a_{kD} = a_k b, a_{cD} = a_c b,$$

$$B_D = p_D\frac{S_D a_{cD}e^{a_{kD}(\psi_{kD}-\psi_{aD})}}{t_s K_D r_D^2},\ S_D = S_y/S,\ \psi_{kD} = \psi_k/b,\ \psi_{aD} = \psi_a/b,$$

$$\delta_{1D,2D} = \delta_{1,2}b = \frac{\kappa_D \mp \sqrt{\kappa_D^2 + 4(B_D+y^2)}}{2}, n = \sqrt{\frac{a_{kD}^2+4y^2}{\lambda_D^2}}$$

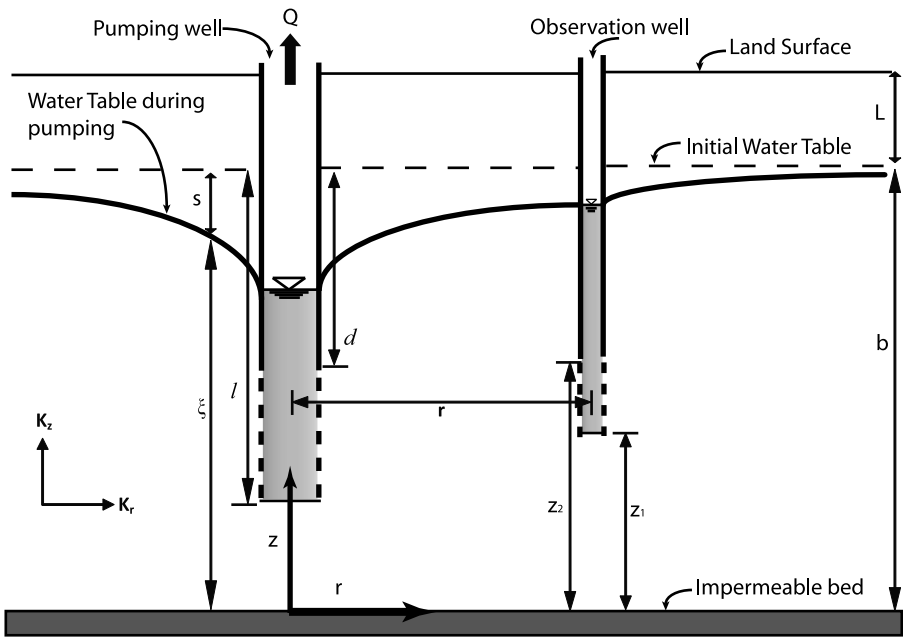

Figure 1. Schematic representation of system geometry.

are dimensionless quantities, p being the parameter of the Laplace transform, and

$$\chi = \begin{cases} -\dfrac{(a_{kD}+n\lambda_D)J_n[i\phi(L_D)] - 2i\sqrt{B_D e^{\lambda_D L_D}}J_{n+1}[i\phi(L_D)]}{(a_{kD}+n\lambda_D)Y_n[i\phi(L_D)] - 2i\sqrt{B_D e^{\lambda_D L_D}}Y_{n+1}[i\phi(L_D)]} & a_{kD} \neq a_{cD} \\ i & a_{kD} \neq a_{cD}, L_D \to \infty \\ -\dfrac{\delta_{1D}}{\delta_{2D}} e^{(\delta_{1D}-\delta_{2D})L_D} & a_{kD} = a_{cD} = \kappa_D \\ 0 & a_{kD} = a_{cD} = \kappa_D, L_D \to \infty \end{cases} \tag{25}$$

$$qb = \begin{cases} \left(\dfrac{a_{kD}}{2} + \dfrac{n\lambda_D}{2}\right) - i\sqrt{B_D}\dfrac{J_{n+1}[i\phi(0)] + \chi Y_{n+1}[i\phi(0)]}{J_n[i\phi(0)] + \chi Y_n[i\phi(0)]} & a_{kD} \neq a_{cD} \\ \dfrac{\delta_{1D} + \chi\delta_{2D}}{1+\chi} & a_{kD} = a_{cD} = \kappa_D \\ \delta_{1D} & a_{kD} = a_{cD} = \kappa_D, L_D \to \infty \end{cases} \tag{26}$$

where $L_D = L/b$, J_n and Y_n being Bessel functions of first and second kind, respectively, of order n.

[10] The corresponding time domain functions s_U and σ are evaluated numerically using the inverse Laplace algorithm of *Crump* [1976] as modified by *de Hoog et al.* [1982]. Whereas standard inversion with respect to p is done over a time interval $[0,t]$ we do the inversion with respect to p_D over a unit dimensionless time (corresponding to p_D^{-1}) interval [0,1], regardless of what t_s is.

2.3. Vertically Averaged Dimensionless Drawdown in Piezometer or Observation Well

[11] Dimensionless drawdown in a piezometer or observation well that penetrates the saturated zone between elevations $z_{D1} = z_1/b$ and $z_{D2} = z_2/b$ (Figure 1) is obtained by averaging the point dimensionless drawdown over this interval according to

$$s_D(r_D, z_{D2} - z_{D1}, t_s) = \frac{1}{z_{D2} - z_{D1}} \int_{z_{D1}}^{z_{D2}} s_D(r_D, z_D, t_s)\, dz_D. \tag{27}$$

3. Theoretical Drawdown Behavior

[12] To investigate the manner in which dimensionless drawdown varies with dimensionless time and space we consider for illustrative purposes a well of zero radius penetrating the upper 60% of the saturated zone ($d_d = 0.0$ and $l_d = 0.6$) of an isotropic aquifer ($K_D = 1$) with a ratio $S/S_y = 1/100$ between storativity and specific yield. The

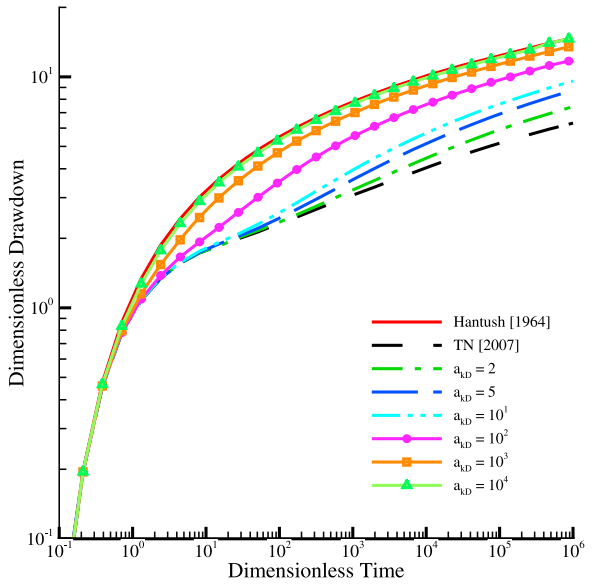

Figure 2. Dimensionless drawdown versus dimensionless time at $r/b = 0.5$ and $z/b = 0.5$ in saturated zone for various values of a_{kD} when $a_{cD} = 1$, $\psi_{kD} - \psi_{aD} = 0$, $K_D = 1$, $S/S_y = 1/100$, $L_D \rightarrow \infty$, $d_D = 0.0$, and $l_D = 0.06$.

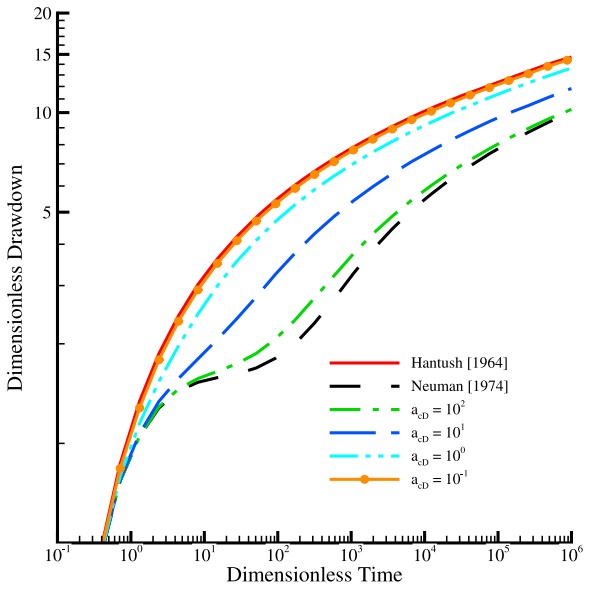

Figure 3. Dimensionless drawdown versus dimensionless time at $r/b = 0.5$ and $z/b = 0.5$ in saturated zone for various values of a_{cD} when $a_{kD} = 10^3$, $\psi_{kD} - \psi_{aD} = 0$, $K_D = 1$, $S/S_y = 1/100$, $L_D \rightarrow \infty$, $d_D = 0.0$, and $l_D = 0.06$.

impacts of varying these parameters are similar to those noted by *Tartakovsky and Neuman* [2007] and we therefore do not discuss them here.

3.1. Time Drawdown Behavior in Saturated Zone

[13] In the saturated zone we plot dimensionless drawdown $s_D = 4\pi Ts/Q$ versus dimensionless time $t_s = \alpha_s t/r^2$ on log-log scale at dimensionless elevation $z/b = 0.5$ and dimensionless radial distance $r/b = 0.5$ from the pumping well.

[14] Figure 2 shows how s_D varies with t_s for various values of a_{kD} when $a_{cD} = 1$, $\psi_{kD} - \psi_{aD} = 0$ and $L_D \rightarrow \infty$. When $a_{kD} = a_{cD} = 1$, our solution reduces to that of *Tartakovsky and Neuman* [2007] as expected given that $\psi_{kD} = \psi_{aD}$. As a_{kD} increases the hydraulic conductivity of the unsaturated zone decreases at an increasingly fast rate as pressure head drops (becomes more negative) relative to its threshold, ψ_k. The rate at which water drains under a given hydraulic gradient out of the unsaturated zone into the saturated zone diminishes, causing dimensionless drawdown in the saturated zone to increase relative to values predicted by *Tartakovsky and Neuman* [2007]. At very large a_{kD} unsaturated conductivity drops precipitously as pressure head falls below ψ_k, causing the unsaturated zone to be effectively impermeable. Hence the aquifer behaves as if it was confined and our solution reduces to that developed for such an aquifer by *Hantush* [1964].

[15] Figure 3 depicts the variation of s_D with t_s for various values of a_{cD} when $a_{kD} = 10^3$, $\psi_{kD} - \psi_{aD} = 0$ and $L_D \rightarrow \infty$. When both exponents are large, hydraulic conductivity and pressure head in the unsaturated zone drop (the latter becoming negative) precipitously as pressure head approaches the thresholds ψ_k and ψ_{cD}, respectively. The unsaturated zone loses its ability to store water above the water table, causing this surface to behave as a moving boundary. Consequently, our solution reduces to that of *Neuman* [1974] for a free surface. As a_{cD} decreases, the capacity of the unsaturated zone to store water at a given negative pressure head increases, causing delayed water table response *a la* Neuman to diminish and dimensionless drawdown to increase earlier than predicted by this author.

[16] Figure 4 illustrates the effect of varying dimensionless unsaturated zone thickness, $L_D = L/b$, on dimensionless time-drawdown when $a_{kD} = a_{cD} = 10$ and $\psi_{kD} - \psi_{aD} = 0$. As long as $L_D \geq 0.25$ ($L \geq 0.25b$), unsaturated zone thickness has no discernible effect on dimensionless drawdown at r/b

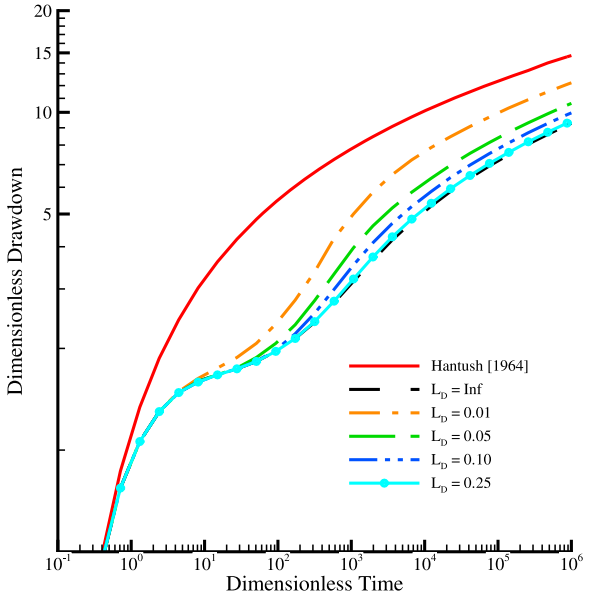

Figure 4. Dimensionless drawdown versus dimensionless time at $r/b = 0.5$ and $z/b = 0.5$ in saturated zone for various values of L_D when $a_{kD} = a_{kD} = 10$, $\psi_{kD} - \psi_{aD} = 0$, $K_D = 1$, $S/S_y = 1/100$, $d_D = 0.0$, and $l_D = 0.6$.

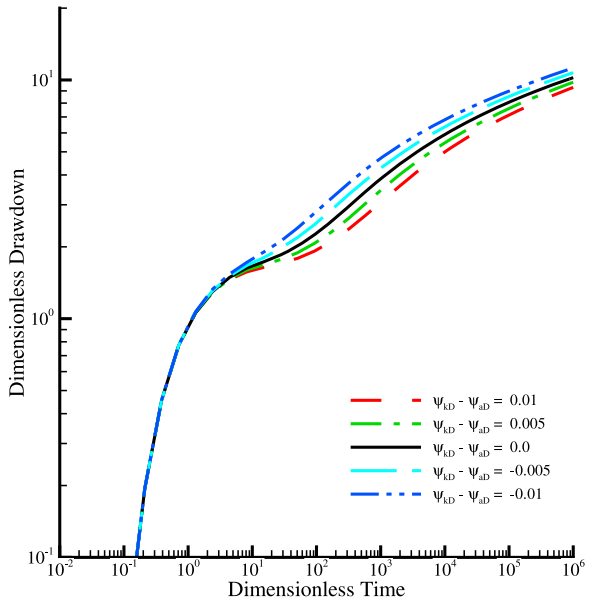

Figure 5. Dimensionless drawdown versus dimensionless time at $r/b = 0.5$ and $z/b = 0.5$ in saturated zone for various values of $\psi_{kD} - \psi_{aD}$ when $a_{kD} = 10^2$, $a_{cD} = 10^1$, $K_D = 1$, $S/S_y = 1/100$, $L_D \rightarrow \infty$, $d_D = 0.0$, and $l_D = 0.6$.

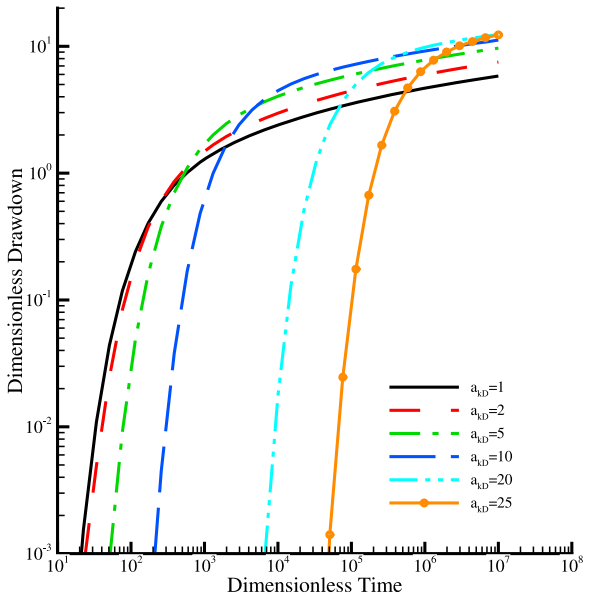

Figure 6. Dimensionless drawdown versus dimensionless time at $r/b = 0.5$ and $z/b = 1.5$ in unsaturated zone for various values of a_{kD} when $a_{cD} = 1$, $\psi_{kD} - \psi_{aD} = 0$, $K_D = 1$, $S/S_y = 1/100$, $L_D \rightarrow \infty$, $d_D = 0.0$, and $l_D = 0.06$.

$= 0.5$ and $z/b = 0.5$ in the saturated zone. This reflects the fact that conditions in the saturated zone depend more on unsaturated flow close to the water table than on that farther from it. A decrease in L_D below 0.25 reduces the amount of water available for drainage from the unsaturated zone as the water table falls, thereby causing dimensionless drawdown in the saturated zone to increase.

[17] We end this part of our analysis by showing in Figure 5 how varying $\psi_{kD} - \psi_{aD}$ impacts dimensionless time-drawdown when $a_{kD} = 10^2$, $a_{cD} = 10^1$ and $L_D \rightarrow \infty$. As this difference increases above zero, the hydraulic conductivity of the unsaturated zone diminishes relative to that obtained when $\psi_{kD} - \psi_{aD} = 0$. The rate at which water drains under a given hydraulic gradient out of the unsaturated zone into the saturated zone diminishes, causing dimensionless drawdown in the saturated zone to increase as it did in Figure 2. As $\psi_{kD} - \psi_{aD}$ decreases below zero (becomes more negative), the ability of the unsaturated zone to store water above the water table diminishes relative to the case where $\psi_{kD} - \psi_{aD} = 0$. The water table acts more and more as a free surface, exhibiting an increasing degree of delayed water table response a la *Neuman* [1974], as was the case in Figure 3.

3.2. Time Drawdown Behavior in Unsaturated Zone

[18] In the unsaturated zone we plot dimensionless drawdown $s_D = 4\pi T\sigma/Q$ versus dimensionless time $t_s = \alpha_s t/r^2$ on log-log scale at dimensionless elevation $z/b = 1.5$ and dimensionless radial distance $r/b = 0.5$ from the pumping well.

[19] Figure 6 shows how s_D varies with t_s for various values of a_{kD} when $a_{cD} = 1$, $\psi_{kD} - \psi_{aD} = 0$ and $L_D \rightarrow \infty$ (compare with Figure 2 showing the effect of a_{kD} in the saturated zone). As a_{kD} increases the hydraulic conductivity of the unsaturated zone decreases at an increasingly fast rate as pressure head drops (becomes more negative) relative to its threshold, ψ_k. The rate at which water drains under a given hydraulic gradient out of the unsaturated zone into the saturated zone diminishes, causing delay and increase in dimensionless drawdown within the unsaturated zone.

[20] Figure 7 depicts the variation of s_D with t_s for various values of a_{cD} when $a_{kD} = 25$, $\psi_{kD} - \psi_{aD} = 0$ and $L_D \rightarrow \infty$ (compare with Figure 3 showing the effect of a_{cD} in the saturated zone). As a_{cD} decreases, the capacity of the

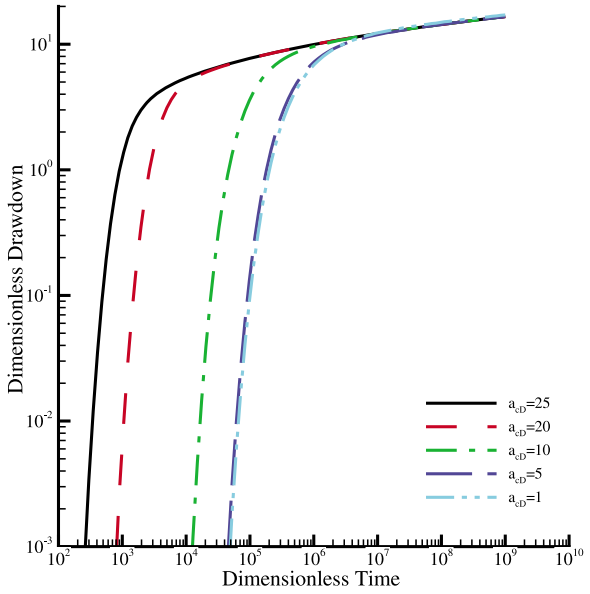

Figure 7. Dimensionless drawdown versus dimensionless time at $r/b = 0.5$ and $z/b = 1.5$ in unsaturated zone for various values of a_{cD} when $a_{kD} = 25$, $\psi_{kD} - \psi_{aD} = 0$, $K_D = 1$, S/S_y 1/100, $L_D \rightarrow \infty$, $d_D = 0.0$, and $l_D = 0.06$.

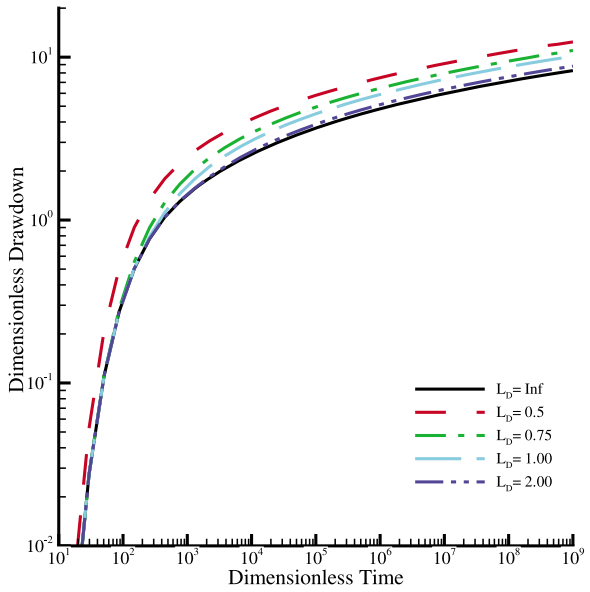

Figure 8. Dimensionless drawdown versus dimensionless time at r/b = 0.5 and z/b = 1.5 in unsaturated zone for various values of L_D when $a_{kD} = a_{cD} = 10$, $\psi_{kD} - \psi_{aD} = 0$, $K_D = 1$, $S/S_y = 1/100$, $d_D = 0.0$, and $l_D = 0.6$.

unsaturated zone to store water at a given negative pressure head increases, causing a delay in the evolution of dimensionless drawdown within the unsaturated zone.

[21] Figure 8 illustrates the effect of varying dimensionless unsaturated zone thickness, $L_D = L/b$, on dimensionless time-drawdown when $a_{kD} = a_{cD} = 10$ and $\psi_{kD} - \psi_{aD} = 0$ (compare with Figure 4 showing the effect of L_D in the saturated zone). As L_D increases from 0.5 to infinity, the amount of water stored in the unsaturated zone goes up and dimensionless drawdown within this zone diminishes.

[22] Figure 9 shows how varying $\psi_{kD} - \psi_{aD}$ impacts dimensionless time-drawdown in the unsaturated zone when $a_{kD} = 10^2$, $a_{cD} = 10^1$ and $L_D \rightarrow \infty$ (compare with Figure 5 showing the effect of $\psi_{kD} - \psi_{aD}$ in the saturated zone). As this difference increases above zero the hydraulic conductivity of, and hence dimensionless drawdown within, the unsaturated zone diminish relative to those obtained when $\psi_{kD} - \psi_{aD} = 0$. Reducing $\psi_{kD} - \psi_{aD}$ below zero (rendering it more negative) brings about a reverse effect.

3.3. Dimensionless Drawdown Profiles

[23] We conclude this analysis by showing in Figure 10 vertical profiles of dimensionless drawdown in the saturated and the unsaturated zones at various values of t_s as functions of a_{kD} and a_{cD} when $\psi_{kD} - \psi_{aD} = 0$, $K_D = 1$, $S/S_y = 1/100$, $L_D \rightarrow \infty$, $d_d = 0.0$ and $l_d = 0.2$ (the pumping well penetrates the upper 20% of the initial saturated thickness). The profiles make clear that dimensionless rate at which dimensionless drawdown propagates from the well into the unsaturated zone diminishes as a_{kD} increases and/or as a_{cD} decreases for reasons discussed earlier.

4. Analysis of Synthetic Aquifer Test

[24] To explore the ability of our solution to (1) reproduce drawdowns predicted by a numerical model that requires fewer simplifying assumptions, and (2) allow inferring saturated and unsaturated aquifer properties from pumping test data, we have conducted a synthetic numerical experiment. The experiment considers a 14 m thick anisotropic aquifer ($K_D = 0.4$) with horizontal hydraulic conductivity $K_r = 1.0 \times 10^{-3}$ m/s, specific storage $S_s = 3.0 \times 10^{-4} m^{-1}$ and specific yield $S_y = 0.322$. Initially, a static water table (defined here as a zero pressure isobar) is situated 7 m below the ground surface. A pumping well discharging at a rate of 60 l/min penetrates the upper 50% of the saturated zone such that $d_d = 0.0$ and $l_d = 0.5$. Water retention and relative hydraulic conductivity are described by the *van Genuchten* [1980]–*Mualem* [1976] constitutive model with parameters α = 0.035 cm^{-1}, $\theta_s = 0.375$, $\theta_r = 0.053$ and $n = 3.18$ typical of sandy soils [*Schaap et al.*, 2001]. Figure A3 shows a least squares fit of our four-parameter exponential models to the latter two, yielding parameter estimates $\psi_a = 14.2$ cm, ψ_k = 8.3 cm, a_k= 8.2 m^{-1} and $a_c = 3.4$ m^{-1}. Figure 11 compares time drawdowns at dimensionless radial distance $r/b = 0.5$ and dimensionless elevation $z/b = 0.5$, obtained numerically with the STOMP code [*White and Oostrom*, 2000] based on van Genuchten-Mualem parameters, with our analytical solution and these best fit parameters. The agreement is good at early and late time values, less good but acceptable at intermediate values.

[25] Figure 12 compares dimensionless time-drawdowns obtained numerically and analytically at dimensionless radial distance $r/b = 0.5$ and elevation $z/b = 1.25$ in the unsaturated zone. The comparison is less good than it was at $z/b = 0.5$ in the saturated zone and deteriorates further as r/b, the dimensionless distance from the pumping well, diminishes (not shown). We attribute this to sharp breaks in our exponential constitutive model at threshold pressure heads ψ_a and ψ_k, not present in the *van Genuchten* [1980]–*Mualem* [1976] model, to which computed drawdowns in

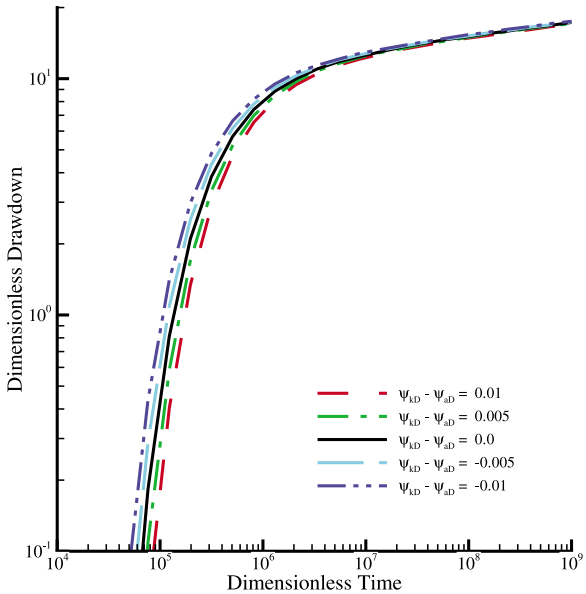

Figure 9. Dimensionless drawdown versus dimensionless time at $r/b = 0.5$ and $z/b = 1.5$ in unsaturated zone for various values of $\psi_{kD} - \psi_{aD}$ when $a_{kD} = 10^2$, $a_{cD} = 10^1$, $K_D = 1$, $S/S_y = 1/100$, $L_D \rightarrow \infty$, $d_D = 0.0$, and $l_D = 0.6$.

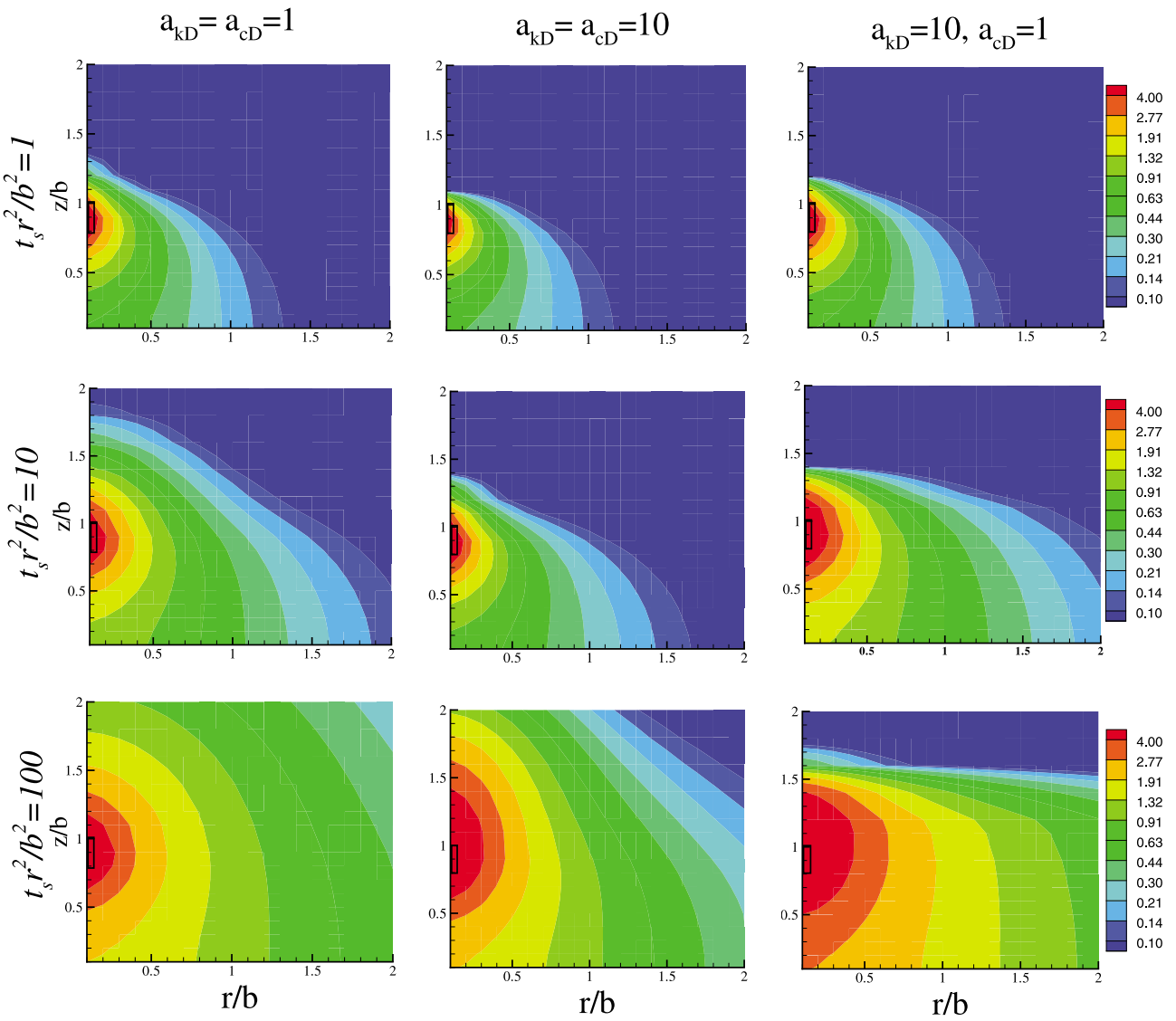

Figure 10. Vertical profiles of dimensionless drawdown in saturated and unsaturated zones at various t_s values corresponding to various values of a_{kD} and a_{cD} when $\psi_{kD} - \psi_{aD} = 0$, $K_D = 1$, $S/S_y = 1/100$, $L_D \rightarrow \infty$, $d_D = 0.0$, and $l_D = 0.2$ (position of pumping well is indicated by rectangle).

the unsaturated zone are more sensitive than those in the saturated zone.

5. Analysis of Cape Cod Aquifer Test

[26] Finally we reanalyze a pumping test conducted by the U.S. Geological Survey in a glacial outwash deposit at Cape Cod, Massachusetts [*Moench et al.*, 2001], using our new solution. The aquifer, composed mainly of sand and gravel deposits estimated to be 51.82 m (170 feet) thick, is bounded from below by fine-grained material of relatively low permeability [*LeBlanc*, 1984; *LeBlanc et al.*, 1986; *Masterson et al.*, 1997]. A well screened 4.02 m (13.2 feet) to 18.35 m (60.2 feet) below the initial water table (defined here, in the absence of information about a capillary fringe, as the traditional zero pressure isobar), located approximately 5.79 m (19 feet) below land surface and 14.26 m (46.8 feet) above mean sea level, was pumped at a constant rate of 0.0202 m^3/s (320 gallons per minute) for 72 h. Hydraulic head responses were monitored in 20 piezometers and observation wells installed at diverse locations, distances and depths around the pumping well. These responses had been analyzed by *Tartakovsky and Neuman* [2007] who presented a layout of the wells and piezometers in their Figures 8 and 9 and listed corresponding completion data in their Table 1.

[27] Water levels in all piezometers and wells were measured manually using a steel tape. In seven piezometers and observation wells (listed in Figure 13), and in the pumping well, water levels were also measured by means of pressure transducers connected to data loggers. We fitted the seven observed records, spanning a time interval of 2 s to 4350 min, simultaneously to our analytical solution by least squares using the parameter estimation code PEST [*Doherty*, 1994]. The result of this fit are presented in Figure 13 and listed, along with corresponding 95% confidence

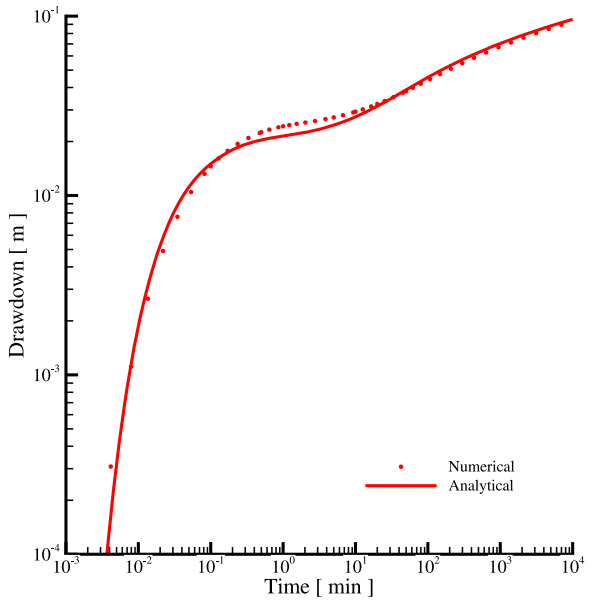

Figure 11. Comparison of numerical (based on van Genuchten-Mualem model) and analytical (based on exponential model) time drawdowns, represented by dots and solid curve, respectively, in saturated zone at $r/b = 0.5$ and $z/b = 0.5$ in synthetic case.

intervals, in Table 1. All but two (F504-060 and F377-037) of the seven records lag behind the fitted theoretical curves at early time. *Moench* [2004], and in the case of one record *Mathias and Butler* [2006], were able to match early time data better, a fact attributed by these authors to their consideration of pumping well storage. In our opinion, it is

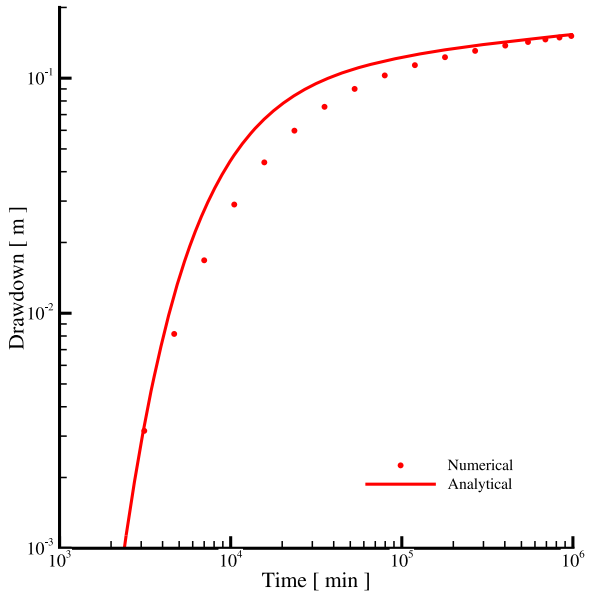

Figure 12. Comparison of numerical (based on van Genuchten-Mualem model) and analytical (based on exponential model) time drawdowns, represented by dots and solid curve, respectively, in unsaturated zone at $r/b = 0.5$ and $z/b = 1.25$ in synthetic case.

Table 1. Parameter Estimates and Their 95% Confidence Limits Obtained by Fitting Our Solution to Seven Transducer-Measured Drawdown Records From Observation Wells and Piezometers

Parameters	Estimated Value	95% Confidence Limit	
		Lower	Upper
K_r (m/s)	1.21×10^{-3}	1.19×10^{-3}	1.23×10^{-3}
K_D	0.53	0.51	0.55
S_s (1/m)	1.05×10^{-4}	9.78×10^{-5}	1.14×10^{-4}
S_y	0.28	0.26	0.30
a_k (1/m)	0.37	0.23	0.60
a_c (1/m)	2.95	1.66	5.23
$\psi_a - \psi_k$ (cm)	1.78	0.08	37.59

equally if not more likely that the early time lag is due to delayed response of the observation wells and piezometers which, given corresponding slug-test data, should be easy to correct in a manner described by *Neuman and Gardner* [1989]. Table 2 lists parameters obtained by *Moench et al.* [2001] and *Tartakovsky and Neuman* [2007] based on all recorded drawdowns and compares them to the estimates of parameters in this study. Whereas our estimates of hydraulic conductivity and specific storage are similar to those obtained by the above authors, our specific yield estimate of 0.28 is slightly higher than the 0.26 value obtained by *Moench et al.* [2001] and significantly higher than the 0.18 value obtained by *Tartakovsky and Neuman* [2007]. Laboratory measurements on six shallow glacial outwash cores at the U.S. Geological Survey Toxic-Substances Hydrology research site at Cape Cod, Massachusetts, by *Mace et al.* [1998] suggest $\theta_s \simeq 0.35$ (see their Figure 6) and $\theta_r \simeq 0 - 0.18$, yielding a range of specific yield values $S_y \simeq 0.17 - 0.35$ that covers the spectrum of the above results.

[28] Our estimates of exponential constitutive model parameters $a_c = 0.37 m^{-1}$, $a_k = 2.95\ m^{-1}$ and $\psi_a - \psi_k = 1.78$ cm in Table 1 provide a least squares fit to a *van Genuchten*

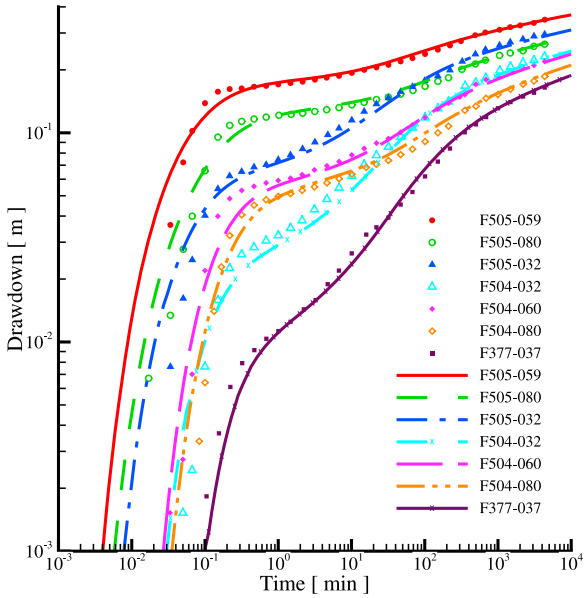

Figure 13. Simultaneous least squares fit of our solution (curves) to seven water level records (symbols) at Cape Cod measured by means of transducers.

Table 2. Parameter Estimates Obtained by Fitting Our Solution to Seven Transducer-Measured Drawdown Records From Observation Wells and Piezometers Compared With Estimates Obtained by *Moench et al.* [2001] and *Tartakovsky and Neuman* [2007] Based on All Measured Drawdowns

	K_r (m/s)	K_z (m/s)	S_s (m^{-1})	S_y	a_c(m^{-1})	a_k(m^{-1})	$\psi_a - \psi_k$(cm)
Moench et al. [2001]	1.17×10^{-3}	7.11×10^{-4}	4.27×10^{-5}	0.26	…	…	…
Tartakvosky et al. [2007]	1.02×10^{-3}	8.13×10^{-4}	9.84×10^{-5}	0.18	$\kappa = a_k = a_c = 0.159$	$\kappa = a_k = a_c = 0.159$	…
This study	1.21×10^{-3}	6.42×10^{-4}	1.05×10^{-4}	0.28	0.37	2.95	1.78

[1980]–*Mualem* [1976] model, shown in Figure 14, with parameters $\psi_a = 8.91$ cm, $\psi_k = 7.13$ cm, $\alpha = 0.0095$ cm^{-1} and $n = 2.10$. An alternative is to rely on the relationships

$$\alpha \approx \frac{a_k}{1.3n}, \qquad \psi_k \approx \frac{1-(n/2)^{-1.163}}{\alpha} \qquad \text{for } n > 2 \qquad (28)$$

proposed by *Ghezzehei et al.* [2007] between parameters of the *Gardner* [1958] and *van Genuchten* [1980]–*Mualem* [1976] relative permeability models. Given $\psi_a - \psi_k$ and a_k, (28) requires estimating only one additional parameter, n, by a least squares fit of our four parameter exponential model to that of van Genuchten and Mualem. The corresponding parameter estimates $\psi_a = 7.39$ cm, $\psi_k = 5.61$ cm, $\alpha = 0.011$ cm^{-1} and $n = 2.11$ are very close to those obtained without the use of (28). Our pumping test estimates $\alpha \simeq 0.01$ cm^{-1} and $n \simeq 2.1$ are smaller than average values $\alpha = 0.24$ cm^{-1} and $n = 2.6$, respectively, of corresponding results from laboratory infiltration tests on the above six shallow glacial outwash cores by *Mace et al.* [1998, Table 2].

[29] Figure 15 compares manually measured drawdowns in 13 wells and piezometers (other than those used for calibration) with those predicted by our analytical solution using the parameter estimates in Table 1 (based on transducer measurements at seven other sites). The fit to all but early time data, which tend to be somewhat scattered (likely due to difficulties in measuring such data accurately with a steel tape), is remarkably good.

6. Conclusions

[30] Our paper leads to the following major conclusions:

[31] 1. Published solutions for saturated-unsaturated flow to a partially penetrating well in a compressible unconfined aquifer indicate (1) the development of significant horizontal hydraulic gradients above the water table and (2) a need to represent more closely empirically established constitutive relationships between pressure head, relative hydraulic conductivity and water content. We developed a new analytical solution that adds two constitutive parameters to that proposed earlier by *Tartakovsky and Neuman* [2007] while allowing the thickness of the unsaturated zone to be finite. Our solution accounts for horizontal unsaturated flow while providing much improved fits to standard constitutive models such as that of *van Genuchten* [1980] and *Mualem* [1976].

[32] 2. Our improved analytical solution for three-dimensional axisymmetric flow to a partially penetrating well in a compressible unconfined aquifer, based on the above exponential constitutive model, generates results that resemble closely those generated by a finite difference code utilizing a corresponding *van Genuchten* [1980]–*Mualem* [1976] model. The correspondence between predicted drawdowns in the unsaturated zone deteriorates with proximity to the pumping well.

[33] 3. Upon reinterpreting seven transducer-measured time-drawdown records from a pumping test conducted by the U.S. Geological Survey at Cape Cod, Massachusetts, using our new solution we found all but two of these records to lag behind the fitted theoretical curves at early time. *Moench* [2004], and in the case of one record *Mathias and Butler* [2006], were able to match early time data better, a fact attributed by these authors to their consideration of pumping well storage. In our opinion, it is equally if not more likely that the early time lag is due to delayed response of the observation wells and piezometers which, given corresponding slug-test data, should be easy to correct in a manner described by *Neuman and Gardner* [1989].

[34] 4. Our reinterpretation of the above seven records has yielded a specific yield estimate of 0.28 that is slightly higher than the 0.26 value obtained by *Moench et al.* [2001] and significantly higher than the 0.18 value obtained using a two-parameter exponential constitutive model by *Tartakovsky and Neuman* [2007]. Laboratory measurements on six shallow glacial outwash cores at Cape Cod by *Mace et al.* [1998]

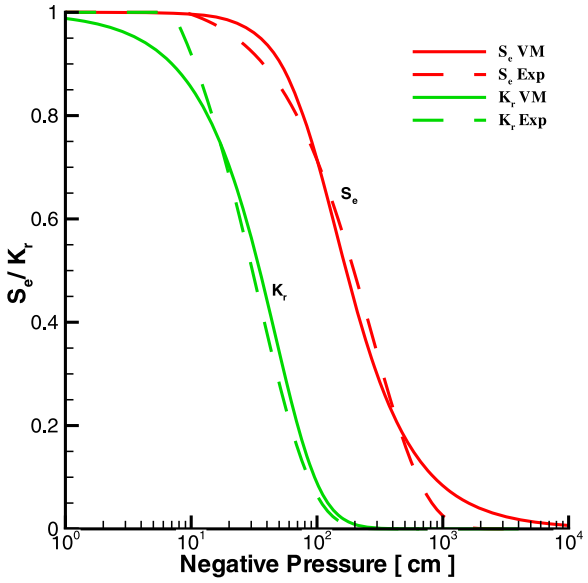

Figure 14. Least squares fit of our exponential constitutive model with parameters $a_c = 0.37$ m^{-1}, $a_k = 2.95$ m^{-1} and $\psi_a - \psi_k = 1.78$ cm to *van Genuchten* [1980]–*Mualem* [1976] model with parameters $\psi_a = 8.91$ cm, $\psi_k = 7.13$ cm, $\alpha = 0.95$ m^{-1}, and $n = 2.1$.

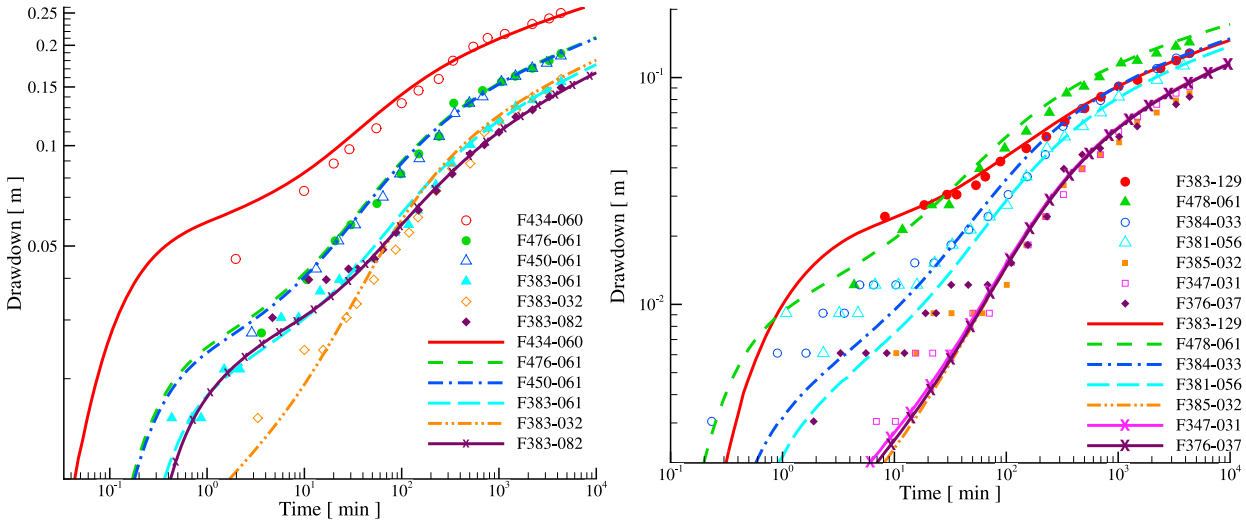

Figure 15. Comparison of manually measured drawdowns (symbols) in 13 wells and piezometers (other than those used for calibration) with those predicted by our analytical solution (curves) using the parameter estimates in Table 1 (based on transducer measurements in seven other piezometers).

suggest a range of specific yield values, $S_y \simeq 0.17 - 0.35$, that covers the spectrum of the above results.

[35] 5. The same reinterpretation has yielded *van Genuchten* [1980]–*Mualem* [1976] parameter estimates $\alpha \simeq 0.01$ cm^{-1} and $n \simeq 2.1$ for the glacial outwash aquifer at Cape Cod. Our pumping test estimates are smaller than average values $\alpha = 0.24$ cm^{-1} and $n = 2.6$, respectively, of corresponding results from laboratory infiltration tests on the above six shallow glacial outwash cores by *Mace et al.* [1998, Table 2].

[36] 6. We have successfully validated our analytical solution with estimates of saturated and unsaturated hydraulic parameters obtained on the basis of seven transducer-measured drawdown records by using them to reproduce with reasonable fidelity drawdown records measured manually in 13 other piezometers and observation wells at Cape Cod.

Appendix A: Four-Parameter Exponential Representation of Constitutive Relationships

[37] It is common to describe moisture retention and relative hydraulic conductivity using constitutive models such as those of *Gardner* [1958] and *Russo* [1988], *Brooks and Corey* [1964], or *van Genuchten* [1980] and *Mualem* [1976]. According to the latter model

$$S_e(\psi) = [1 + (\alpha\psi)^n]^{1/n-1} \tag{A1}$$

$$k(\psi) = S_e(\psi)^{1/2}\left\{1 - \left[1 - S_e(\psi)^{n/(n-1)}\right]^{1-1/n}\right\}^2 \tag{A2}$$

where $n > 0$ is a dimensionless parameter and $\alpha > 0$ has dimensions of inverse length. As aquifers often consist of sandy material, we consider the parameters $\alpha = 0.035$ cm^{-1} and $n = 3.18$ typical of sandy soils [*Schaap et al.*, 2001].

Figure A1 shows a best fit of the two-parameter exponential model used by *Tartakovsky and Neuman* [2007] to (A1) and (A2) with these parameters, the estimates being $\psi_a = 9.8$ cm and $a_c = 5.2$ m^{-1}; Figure A2 shows a similar fit of the three-parameter exponential model used by *Mathias and Butler* [2006] with estimates $\psi_a = 10.5$ cm, $a_k = 12.4$ m^{-1} and $a_c = 3.2$ m^{-1}; and Figure A3 depicts a best fit of our four-parameter exponential model to the same with estimates $\psi_a = 14.2$ cm, $\psi_k = 8.3$ cm, $a_k = 8.2$ m^{-1} and $a_c = 3.4$ m^{-1}.

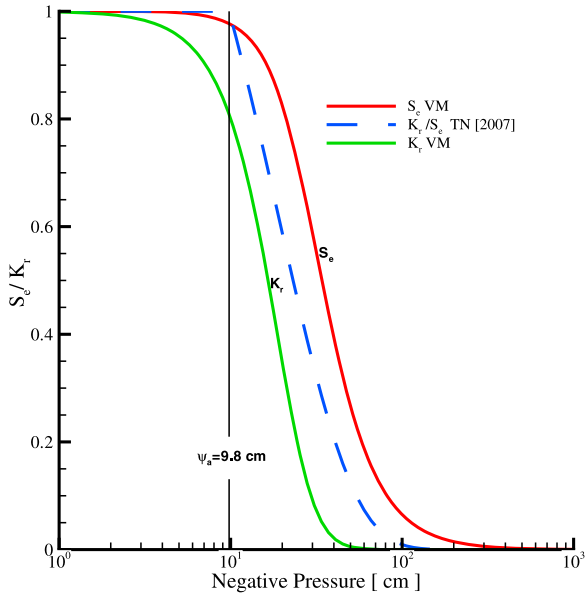

Figure A1. Best fit of two−parameter exponential model used by *Tartakovsky and Neuman* [2007] (blue) to *van Genuchten* [1980] (red) and *Mualem* [1976] (green) model with $\alpha = 0.035$ cm^{-1} and $n = 3.18$ typical of sandy soils [*Schaap et al.*, 2001].

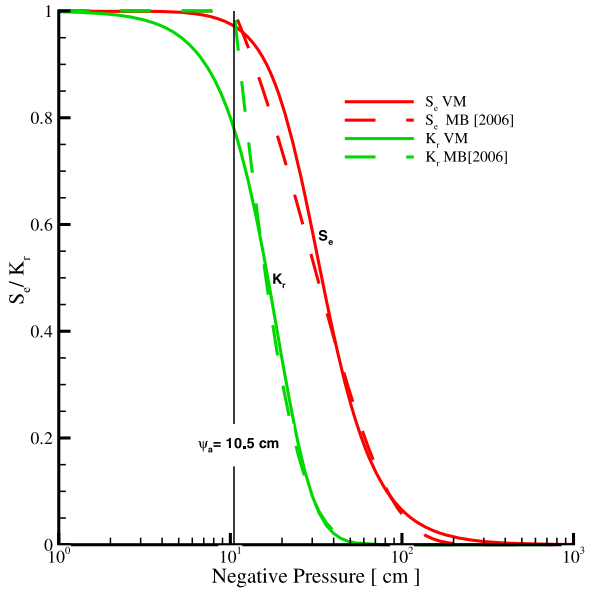

Figure A2. Best fit of three-parameter exponential model used by *Mathias and Butler* [2006] (dashed lines) to *van Genuchten* [1980] (red) and *Mualem* [1976] (green) model, respectively, with $\alpha = 0.035$ cm^{-1} and $n = 3.18$ typical of sandy soils [*Schaap et al.*, 2001].

One observes a progressive improvement in these fits as the number of parameters increases from 2 to 4.

Appendix B: Decomposition of Saturated Zone Solution

[38] In a manner analogous to *Neuman* [1974] and *Tartakovsky and Neuman* [2007] we decompose s into two parts

$$s = s_H + s_U \tag{B1}$$

where s_H is *Hantush*'s [1964] solution for a partially penetrating well in a confined aquifer, satisfying

$$\frac{1}{r}\frac{\partial}{\partial r}\left(r\frac{\partial s_H}{\partial r}\right) + K_D\frac{\partial^2 s_H}{\partial z^2} = \frac{1}{\alpha_s}\frac{\partial s_H}{\partial t} \qquad 0 \le z < b \tag{B2}$$

$$s_H(r,z,0) = 0 \tag{B3}$$

$$s_H(\infty,z,t) = 0 \tag{B4}$$

$$\frac{\partial s_H}{\partial z} = 0 \qquad z = 0 \text{ and } z = b \tag{B5}$$

$$\lim_{r\to 0}\frac{\partial s_H}{\partial r} = 0 \qquad 0 \le z \le b - l \qquad b - d \le z \le b \tag{B6}$$

$$\lim_{r\to 0} r\frac{\partial s_H}{\partial r} = -\frac{Q}{2\pi K_r(l-d)} \qquad b - l \le z \le b - d. \tag{B7}$$

and s_U is a correction due to saturated-unsaturated unconfined conditions, satisfying

$$\frac{1}{r}\frac{\partial}{\partial r}\left(r\frac{\partial s_U}{\partial r}\right) + K_D\frac{\partial^2 s_U}{\partial z^2} = \frac{1}{\alpha_s}\frac{\partial s_U}{\partial t} \qquad 0 \le z < b \tag{B8}$$

$$s_U(r,z,0) = 0 \tag{B9}$$

$$s_U(\infty,z,t) = 0 \tag{B10}$$

$$\frac{\partial s_U}{\partial z} = 0 \qquad z = 0 \tag{B11}$$

$$\lim_{r\to 0}\frac{\partial s_U}{\partial r} = 0 \qquad 0 \le z \le b \tag{B12}$$

subject to interface conditions (13) and (14) written as

$$s_H + s_U - \sigma = 0 \qquad z = b \tag{B13}$$

$$\frac{\partial s_H}{\partial z} + \frac{\partial s_U}{\partial z} - \frac{\partial \sigma}{\partial z} = 0 \qquad z = b. \tag{B14}$$

Appendix C: Laplace Space Solution for Saturated Zone

[39] Equations (B1)–(B14) are solved by sequential application of the Hankel transform

$$f(a) = \int_0^\infty rJ_o(ar)f(r)dr \tag{C1}$$

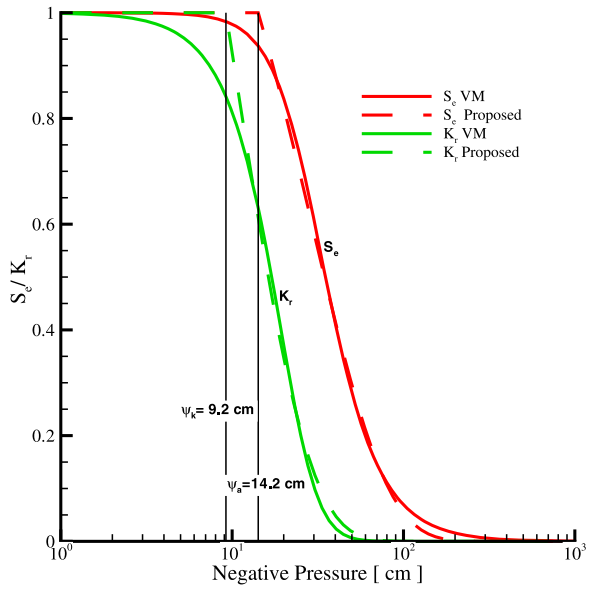

Figure A3. Best fit of four-parameter exponential model proposed in this paper (dashed lines) to *van Genuchten* [1980] (red) and *Mualem* [1976] (green) model, respectively, with $\alpha = 0.035$ cm^{-1} and $n = 3.18$ typical of sandy soils [*Schaap et al.*, 2001].

and Laplace transform

$$f(p) = \int_0^\infty f(t)e^{-pt}dt \tag{C2}$$

with Hankel parameter a and Laplace parameter p, J_0 being zero-order Bessel function of the first kind.

[40] *Neuman* [1974] showed that the double transform of Hantush's solution is

$$\bar{\bar{s}}_H = \frac{Q}{2\pi TK_D p}\left[\frac{1}{\eta^2} + \frac{2}{\pi(l_D - d_D)}\sum_{n=1}^{\infty}\frac{1}{n}\cos[n\pi(1 - z_D)] \cdot [\sin(n\pi l_D) - \sin(n\pi d_D)]\frac{1}{\eta^2 + n^2\pi^2/b^2}\right] \tag{C3}$$

where $\eta^2 = a^2/K_D + p/\alpha_s K_D$. The Laplace transform of (B8)–(B14) is

$$\frac{1}{r}\frac{\partial}{\partial r}\left(r\frac{\partial \bar{s}_U}{\partial r}\right) + K_D\frac{\partial^2 \bar{s}_U}{\partial z^2} = \frac{p}{\alpha_s}\bar{s}_U \qquad 0 \le z < b \tag{C4}$$

$$\bar{s}_U(\infty, z, p) = 0 \tag{C5}$$

$$\frac{\partial \bar{s}_U}{\partial z} = 0 \qquad z = 0 \tag{C6}$$

$$\lim_{r\to 0}\frac{\partial \bar{s}_U}{\partial r} = 0 \qquad 0 \le z \le b \tag{C7}$$

$$\bar{s}_H + \bar{s}_U - \bar{\sigma} = 0 \qquad z = b \tag{C8}$$

$$\frac{\partial \bar{s}_H}{\partial z} + \frac{\partial \bar{s}_U}{\partial z} - \frac{\partial \bar{\sigma}}{\partial z} = 0 \qquad z = b. \tag{C9}$$

[41] Taking the Hankel transform of (C4)–(C9) and using the relationship [e.g., *Neuman*, 1974]

$$H\left\{\frac{1}{r}\frac{\partial}{\partial r}\left(r\frac{\partial \bar{s}_U}{\partial r}\right)\right\} = -a^2\bar{\bar{s}}_U - \lim_{r\to 0} r\frac{\partial \bar{s}_U}{\partial r} \tag{C10}$$

yields

$$-a^2\bar{\bar{s}}_U + K_D\frac{\partial^2 \bar{\bar{s}}_U}{\partial z^2} = \frac{p}{\alpha_s}\bar{\bar{s}}_U \qquad 0 \le z < b \tag{C11}$$

$$\frac{\partial \bar{\bar{s}}_U}{\partial z} = 0 \qquad z = 0 \tag{C12}$$

$$\bar{\bar{s}}_H + \bar{\bar{s}}_U - \bar{\bar{\sigma}} = 0 \qquad z = b \tag{C13}$$

$$\frac{\partial \bar{\bar{s}}_H}{\partial z} + \frac{\partial \bar{\bar{s}}_U}{\partial z} - \frac{\partial \bar{\bar{\sigma}}}{\partial z} = 0 \qquad z = b. \tag{C14}$$

[42] The general solution of (C11) subject to (C12) is

$$\bar{\bar{s}}_U = \rho\cosh(\eta z) \tag{C15}$$

where ρ is a constant. Considering that $\left(\partial\bar{\bar{s}}_H/\partial z\right)_{z=b} = 0$ by virtue of (B5) and that

$$\left(\frac{\partial \bar{\bar{\sigma}}}{\partial z}\right)_{z=b} = q\left(\bar{\bar{s}}_H + \bar{\bar{s}}_U\right)_{z=b} \tag{C16}$$

which, together with q, are derived in (D15) we obtain from (C14) and (C15)

$$\bar{\bar{s}}_U = -\left(\bar{\bar{s}}_H\right)_{z=b}\frac{\cosh(\eta z)}{\cosh(\eta b) - \frac{\eta}{q}\sinh(\eta b)}. \tag{C17}$$

[43] From (C3) it follows that

$$\left(\bar{\bar{s}}_H\right)_{z=b} = \frac{Q}{2\pi TK_D p}\left[\frac{1}{\eta^2} + \frac{2}{\pi(l_D - d_D)}\sum_{n=1}^{\infty}\frac{1}{n} \cdot [\sin(n\pi l_D) - \sin(n\pi d_D)]\frac{1}{\eta^2 + n^2\pi^2/b^2}\right] \tag{C18}$$

which, according to *Neuman* [1974, p. 309], can be rewritten as

$$\left(\bar{\bar{s}}_H\right)_{z=b} = -\frac{Q}{2\pi TK_D p}\left[\frac{\sinh[b\eta(1 - l_D)] - \sinh[b\eta(1 - d_D)]}{\eta^2(l_D - d_D)\sinh(b\eta)}\right]. \tag{C19}$$

[44] Substituting (C19) in (C17) gives

$$\bar{\bar{s}}_U = \frac{Q}{2\pi TK_D p}\frac{\cosh(\eta z)}{\cosh(\eta b) - \frac{\eta}{q}\cosh(\eta b)} \cdot \left[\frac{\sinh[b\eta(1 - l_D)] - \sinh[b\eta(1 - d_D)]}{\eta^2(l_D - d_D)\sinh(b\eta)}\right] \tag{C20}$$

[45] The inverse Hankel transform of (C20) is

$$\bar{s}_U = \frac{Q}{2\pi TK_D p}\int_0^\infty \frac{\cosh(\eta z)}{\cosh(\eta b) - \frac{\eta}{q}\cosh(\eta b)} \cdot \left[\frac{\sinh[b\eta(1 - l_D)] - \sinh[b\eta(1 - d_D)]}{\eta^2(l_D - d_D)\sinh(b\eta)}\right] aJ_0(ar)da \tag{C21}$$

[46] Defining a new variable $y = ar/K_D^{1/2}r_D$ transforms (C21) into (23).

Appendix D: Laplace Space Solution for Unsaturated Zone

D1. General Solution

[47] The Laplace transformation of (7) and (9)–(12) is

$$k_0(z)\frac{1}{r}\frac{\partial}{\partial r}\left(r\frac{\partial \bar{\sigma}}{\partial r}\right) + K_D\frac{\partial}{\partial z}\left(k_0(z)\frac{\partial \bar{\sigma}}{\partial z}\right) = p\frac{C_0(z)}{K_r}\bar{\sigma} \qquad b < z < b + L \tag{D1}$$

$$\bar{\sigma}(\infty, z, p) = 0 \tag{D2}$$

$$\frac{\partial\overline{\sigma}}{\partial z}=0 \qquad z=b+L \tag{D3}$$

$$\lim_{r\to 0} r\frac{\partial\overline{\sigma}}{\partial r}=0 \qquad b<z<b+L. \tag{D4}$$

[48] The Hankel transform of (D1)–(D4) considering (C10) and (17)–(18) is

$$-a^2\overline{\overline{\sigma}}+K_D\frac{\partial^2\overline{\overline{\sigma}}}{\partial z^2}-K_D a_k\frac{\partial\overline{\overline{\sigma}}}{\partial z}=p\frac{S_y a_c e^{a_k(\psi_k-\psi_a)}}{K_r}e^{(a_k-a_c)(z-b)}\overline{\overline{\sigma}} \qquad b\le z\le b+L \tag{D5}$$

$$\frac{\partial\overline{\overline{\sigma}}}{\partial z}=0 \qquad z=b+L \tag{D6}$$

[49] Equation (D5) can be rearranged as

$$\frac{\partial^2\overline{\overline{\sigma}}}{\partial z^2}-a_k\frac{\partial\overline{\overline{\sigma}}}{\partial z}-\left(Be^{\lambda(z-b)}+C\right)\overline{\overline{\sigma}}=0 \qquad b\le z\le b+L \tag{D7}$$

where $\lambda=a_k-a_c$, $B=p[(S_y a_c e^{a_k(\psi_k-\psi_a)})/K_r K_D]$ and $C=a^2/K_D$. Its general solution is given by [*Polyanin and Zaitzev*, 2003]

$$\overline{\overline{\sigma}}(z)=e^{a_k(z-b)/2}\{C_1 J_n[i\phi(z-b)]+C_2 Y_n[i\phi(z-b)]\} \tag{D8}$$

where J_n and Y_n are Bessel function of first and second kind, respectively, of order $n=\sqrt{(a_k^2+4C)/\lambda^2}$; $i=\sqrt{-1}$; and $\phi(z)=\sqrt{(4B/\lambda^2)}e^{\lambda z/2}$. Setting $C_2=\chi C_1$ in (D8), substituting into (C13), solving for C_1, substituting the latter into (D8) and using (C17) gives

$$\overline{\overline{\sigma}}(z)=e^{a_k(z-b)/2}\left[1-\frac{\cosh(\eta b)}{\cosh(\eta b)-\frac{\eta}{q}\sinh(\eta b)}\right]\cdot\frac{J_n[i\phi(z-b)]+\chi Y_n[i\phi(z-b)]}{J_n[i\phi(0)]+\chi Y_n[i\phi(0)]}\left(\overline{\overline{s}}_H\right)_{z=b}. \tag{D9}$$

[50] Taking the derivative of (D9) using the identities $dJ_n(z)/dz=nJ_n(z)/z-J_{n+1}(z)$ and $dY_n(z)/dz=nY_n(z)/z-Y_{n+1}(z)$ [*Abramovitz and Stegun*, 1965, p. 439] yields

$$\frac{d\overline{\overline{\sigma}}}{dz}=\left(\frac{a_k}{2}+\frac{n\lambda}{2}\right)\overline{\overline{\sigma}}(z)-i\sqrt{Be^{\lambda(z-b)}}e^{a_k(z-b)/2}\cdot\frac{J_{n+1}[i\phi(z-b)]+\chi Y_{n+1}[i\phi(z-b)]}{J_n[i\phi(0)]+\chi Y_n[i\phi(0)]}\left(\overline{\overline{s}}_H+\overline{\overline{s}}_U\right)_{z=b}. \tag{D10}$$

[51] Substituting (D10) into (D6) gives

$$\chi=-\frac{(a_k+n\lambda)J_n[i\phi(L)]-2i\sqrt{Be^{\lambda L}}J_{n+1}[i\phi(L)]}{(a_k+n\lambda)Y_n[i\phi(L)]-2i\sqrt{Be^{\lambda L}}Y_{n+1}[i\phi(L)]}. \tag{D11}$$

[52] Combining (D10) with (C13) allows writing

$$\left(\frac{d\overline{\overline{\sigma}}}{dz}\right)_{z=b}=q\left(\overline{\overline{s}}_H+\overline{\overline{s}}_U\right)_{z=b} \tag{D12}$$

where

$$q=\left(\frac{a_k}{2}+\frac{n\lambda}{2}\right)-i\sqrt{B}\frac{J_{n+1}[i\phi(0)]+\chi Y_{n+1}[i\phi(0)]}{J_n[i\phi(0)]+\chi Y_n[i\phi(0)]}. \tag{D13}$$

[53] Substituting (C19) in (D9) and taking the inverse Hankel transform of (D9) gives

$$\overline{\sigma}(r,z,p)=\frac{Q}{2\pi TK_D p}\int_0^\infty e^{a_k(z-b)/2}\left[\frac{\cosh(\eta b)}{\cosh(\eta b)-\frac{\eta}{q}\sinh(\eta b)}-1\right]\cdot\frac{J_n[i\phi(z-b)]+\chi Y_n[i\phi(z-b)]}{J_n[i\phi(0)]+\chi Y_n[i\phi(0)]}\cdot\left[\frac{\sinh[b\eta(1-l_D)]-\sinh[b\eta(1-d_D)]}{\eta^2(l_D-d_D)\sinh(b\eta)}\right]rJ_0(ar)\mathrm{d}r \tag{D14}$$

[54] Defining a new variable $y=ar/K_D^{1/2}r_D$ transforms (D14) into the part of (24) corresponding to $a_c\neq a_k$.

D2. Solution for $a_k = a_c$

[55] When $a_k=a_c=\kappa$, (D7) reduces to

$$\frac{\partial^2\overline{\overline{\sigma}}}{\partial z^2}-\kappa\frac{\partial\overline{\overline{\sigma}}}{\partial z}-(B+C)\overline{\overline{\sigma}}=0 \qquad b\le z\le b+L \tag{D15}$$

where $B=p(S_y\kappa e^{\kappa(\psi_k-\psi_a)})/K_r K_D$ and $C=a^2/K_D$. Its general solution is

$$\overline{\overline{\sigma}}=C_1e^{\delta_1(z-b)}+C_2e^{\delta_2 z(z-b)} \tag{D16}$$

where $\delta_{1,2}=(\kappa\mp\sqrt{\kappa^2+4(B+C)})/2$. Setting $C_2=\chi C_1$ and substituting into (C13) gives

$$C_1=\frac{\left(\overline{\overline{s}}_H+\overline{\overline{s}}_U\right)_{z=b}}{1+\chi} \tag{D17}$$

so that (D16) becomes

$$\overline{\overline{\sigma}}=\frac{e^{\delta_1(z-b)}+\chi e^{\delta_2(z-b)}}{1+\chi}\left(\overline{\overline{s}}_H+\overline{\overline{s}}_U\right)_{z=b}. \tag{D18}$$

[56] Substituting this into (D6) gives

$$\chi=-\frac{\delta_1}{\delta_2}e^{(\delta_1-\delta_2)L}. \tag{D19}$$

[57] Evaluating the derivative of (D18) at $z=b$ allows writing

$$\left(\frac{d\overline{\overline{\sigma}}}{dz}\right)_{z=b}=q\left(\overline{\overline{s}}_H+\overline{\overline{s}}_U\right)_{z=b} \tag{D20}$$

where

$$q=\frac{\delta_1+\chi\delta_2}{1+\chi}. \tag{D21}$$

[58] Substituting (C17) into (D18) yields

$$\overline{\overline{\sigma}} = \left[1 - \frac{\cosh(\eta b)}{\cosh(\eta b) - \frac{\eta}{q}\sinh(\eta b)}\right] \frac{e^{\delta_1(z-b)} + \chi e^{\delta_2(z-b)}}{1+\chi} \left(\overline{\overline{s}}_H\right)_{z=b}. \tag{D22}$$

[59] Substituting (C19) and (D22) and taking the inverse Hankel transform results in

$$\overline{\sigma}(r,z,p) = \frac{Q}{2\pi T K_D p}\int_0^\infty \left[\frac{\cosh(\eta b)}{\cosh(\eta b) - \frac{\eta}{q}\sinh(\eta b)} - 1\right] \cdot \frac{e^{\delta_1(z-b)} + \chi e^{\delta_2(z-b)}}{1+\chi} \cdot \left[\frac{\sinh[b\eta(1-l_D)] - \sinh[b\eta(1-d_D)]}{\eta^2(l_D - d_D)\sinh(b\eta)}\right] r J_0(ar)\mathrm{d}r \tag{D23}$$

[60] Defining a new variable $y = ar/K_D^{1/2} r_D$ transforms (D23) into the part of (24) corresponding to $a_c = a_k = \kappa$.

D3. General Solution for Large *L*

[61] For large arguments the Bessel functions can be approximated as

$$J_n(x) \approx \sqrt{\frac{2}{\pi x}}\cos\left[\left\{x - \frac{2n+1}{4}\pi\right\}\right],$$
$$Y_n(x) \approx \sqrt{\frac{2}{\pi x}}\sin\left[\left\{x - \frac{2n+1}{4}\pi\right\}\right] \tag{D24}$$

$$J_{n+1}(x) \approx \sqrt{\frac{2}{\pi x}}\cos\left[\left\{x - \frac{2n+1}{4}\pi\right\} - \frac{\pi}{2}\right],$$
$$Y_{n+1}(x) \approx \sqrt{\frac{2}{\pi x}}\sin\left[\left\{x - \frac{2n+1}{4}\pi\right\} - \frac{\pi}{2}\right] \tag{D25}$$

[62] Considering that cos (θ - (π/2)) = sin (θ) and sin(θ - (π/2)) = -cos(θ) the above imply

$$J_{n+1}(x) \approx Y_n(x), \qquad Y_{n+1}(x) \approx -J_n(x) \tag{D26}$$

[63] Substituting into (D11) gives

$$\chi = -\frac{i\frac{(a_k+n\lambda)}{2\sqrt{Be^{\lambda L}}}J_n[i\phi(L)] + Y_n[i\phi(L)]}{i\frac{(a_k+n\lambda)}{2\sqrt{Be^{\lambda L}}}Y_n[i\phi(L)] - J_n[i\phi(L)]}. \tag{D27}$$

[64] In the limit $L \to \infty$ we obtain, by virtue of (D24) and (D25).

$$\lim_{L\to\infty}\chi = \lim_{L\to\infty}\frac{Y_n[i\phi(L)]}{J_n[i\phi(L)]} = \lim_{L\to\infty}\frac{\sin\left[i\phi(L) - \frac{2n+1}{4}\pi\right]}{\cos\left[i\phi(L) - \frac{2n+1}{4}\pi\right]}$$
$$= \lim_{L\to\infty}\frac{i\sinh[\phi(L)]\cos\left(\frac{2n+1}{4}\pi\right) - \cosh[\phi(L)]\sin\left(\frac{2n+1}{4}\pi\right)}{\cosh[\phi(L)]\cos\left(\frac{2n+1}{4}\pi\right) + i\sinh[\phi(L)]\sin\left(\frac{2n+1}{4}\pi\right)} = i \tag{D28}$$

[65] Substituting (D28) into (D23) yields a general solution for large L.

D4. Solution for Large *L* When $a_c = a_k$

[66] Since (δ_1 - δ_2) in (D19) is always negative, $\chi \to 0$ as $L \to \infty$ and (D23) reduces to

$$\overline{\sigma}(r_D,z,p) = \frac{Q}{2\pi T K_D p}\int_0^\infty \left[\frac{q\eta\sinh(\eta b)}{q\cosh(\eta b) - \eta\sinh(\eta b)}\right] e^{\delta_1(z-b)} \cdot \left[\frac{\sinh[b\eta(1-l_D)] - \sinh[b\eta(1-d_D)]}{\eta^2(l_D - d_D)\sinh(b\eta)}\right] r J_0(ar)\mathrm{d}r \tag{D29}$$

which is identical to (B33) of *Tartakovsky and Neuman* [2007].

[67] **Acknowledgment.** This research was supported in part through a contract with Vanderbilt University under the Consortium of Risk Evaluation with Stakeholder Participation (CRESP) III, funded by the U.S. Department of Energy.

References

Abramovitz, M., and I. A. Stegun (1965), *Handbook of Mathematical Functions*, Dover, Mineola, N. Y.

Brooks, R. H., and A. T. Corey (1964), *Hydraulic Properties of Porous Media*, *Hydrol. Pap. 30*, Colo. State Univ., Fort Collins.

Crump, K. S. (1976), Numerical inversion of Laplace transforms using a Fourier series approximation, *J. ACM*, *23*, 89–96, doi:10.1145/321921.321931.

de Hoog, F. R., J. H. Knight, and A. N. Stokes (1982), An improved method for numerical inversion of Laplace transforms, *SIAM J. Sci. Comput.*, *3*, 357–366, doi:10.1137/0903022.

Doherty, J. (1994), *PEST: Model-Independent Parameter Estimation*, 122 pp., Watermark Comput., Corinda, Qld., Australia.

Gardner, W. R. (1958), Some steady state solutions of unsaturated moisture flow equations with application to evaporation from a water table, *Soil Sci.*, *85*, 228–232, doi:10.1097/00010694-195804000-00006.

Ghezzehei, T. A., T. J. Kneafsey, and G. W. Su (2007), Correspondence of the Gardner and van Genuchten-Mualem relative permeability function parameters, *Water Resour. Res.*, *43*, W10417, doi:10.1029/2006WR005339.

Hantush, M. S. (1964), Hydraulics of wells, *Adv. Hydrosci.*, *1*, 281–442.

Kroszynski, U. I., and G. Dagan (1975), Well pumping in unconfined aquifers: The influence of the unsaturated zone, *Water Resour. Res.*, *11*, 479–490, doi:10.1029/WR011i003p00479.

LeBlanc, D. R. (1984), Sewage plume in a sand and gravel aquifer, Cape Cod, Massachusetts, *U.S. Geol. Surv. Water Supply Pap.*, *2218*, 28 pp.

LeBlanc, D. R., J. H. Guswa, M. H. Frimpter, and C. J. Londquist (1986), Ground-water resources of Cape Cod, Massachusetts, *U.S. Geol. Surv. Hydrol. Atlas*, *HA-692*, 4 plates.

Mace, A., D. L. Rudolph, and R. G. Kachanoski (1998), Suitability of parametric models to describe the hydraulic properties of an unsaturated coarse sand and gravel, *Ground Water*, *36*, 465–475, doi:10.1111/j.1745-6584.1998.tb02818.x.

Masterson, J. P., B. D. Stone, D. A. Walters, and J. Savoie (1997), Hydrogeologic framework of western Cape Cod, Massachusetts, *U.S. Geol. Surv. Hydrol. Atlas*, *HA-741*.

Mathias, S. A., and A. P. Butler (2006), Linearized Richards' equation approach to pumping test analysis in compressible aquifers, *Water Resour. Res.*, *42*, W06408, doi:10.1029/2005WR004680.

Moench, A. F. (1997), Flow to a well of finite diameter in a homogeneous, anisotropic water table aquifer, *Water Resour. Res.*, *33*, 1397–1407, doi:10.1029/97WR00651.

Moench, A. F. (2004), Importance of the vadose zone in analyses of unconfined aquifer tests, *Ground Water*, *42*(2), 223–233, doi:10.1111/j.1745-6584.2004.tb02669.x.

Moench, A. F. (2008), Analytical and numerical analyses of an unconfined aquifer test considering unsaturated zone characteristics, *Water Resour. Res.*, *44*, W06409, doi:10.1029/2006WR005736.

Moench, A. F., S. P. Garabedian, and D. R. LeBlanc (2001), Estimation of hydraulic parameters from an unconfined aquifer test conducted in a

glacial outwash deposit, Cape Cod, Massachusetts, *U.S. Geol. Surv. Prof. Pap.*, *1629*, 69 pp.

Mualem, Y. (1976), A new model for predicting hydraulic conductivity of unsaturated porous media, *Water Resour. Res.*, *12*, 513–522, doi:10.1029/WR012i003p00513.

Neuman, S. P. (1972), Theory of flow in unconfined aquifers considering delayed response of the water table, *Water Resour. Res.*, *8*, 1031–1045, doi:10.1029/WR008i004p01031.

Neuman, S. P. (1974), Effects of partial penetration on flow in unconfined aquifers considering delayed aquifer response, *Water Resour. Res.*, *10*, 303–312, doi:10.1029/WR010i002p00303.

Neuman, S. P., and D. A. Gardner (1989), Determination of aquitard/aquiclude hydraulic properties from arbitrary water level fluctuations by deconvolution, *Ground Water*, *27*(1), 66–76, doi:10.1111/j.1745-6584.1989.tb00009.x.

Polyanin, A. D., and V. F. Zaitsev (2003), *Handbook of Exact Solutions for Ordinary Differential Equations*, 2nd ed., CRC Press, Boca Raton, Fla.

Russo, D. (1988), Determining soil hydraulic properties by parameter estimation: On the selection of a model for the hydraulic properties, *Water Resour. Res.*, *24*(3), 453–459, doi:10.1029/WR024i003p00453.

Schaap, M. G., F. J. Leij, and M. T. van Genuchten (2001), Rosetta: A computer program for estimating soil hydraulic parameters with hierarchical pedotransfer functions, *J. Hydrol.*, *251*, 163–176, doi:10.1016/S0022-1694(01)00466-8.

Tartakovsky, G. D., and S. P. Neuman (2007), Three-dimensional saturated-unsaturated flow with axial symmetry to a partially penetrating well in a compressible unconfined aquifer, *Water Resour. Res.*, *43*, W01410, doi:10.1029/2006WR005153.

Theis, C. V. (1935), The relationship between the lowering of the piezometric surface and rate and duration of discharge of a well using groundwater storage, *Eos Trans. AGU*, *16*, 519–524.

van Genuchten, M. T. (1980), A closed-form equation for predicting the hydraulic conductivity of unsaturated soils, *Soil Sci. Soc. Am. J.*, *44*, 892–898.

White, M. D., and M. Oostrom (2000), STOMP: Subsurface transport over multiple phase: Theory guide, *PNNL-11216(UC-2010)*, Pac. Northwest Natl. Lab., Richland, Wash.

P. K. Mishra and S. P. Neuman, Department of Hydrology and Water Resources, University of Arizona, 1133 E. James E. Rogers Way, Tucson, AZ 85721, USA. (neuman@hwr.arizona.edu)